

Global ocean heat content in the Last Interglacial

S. Shackleton^{1*}, D. Baggenstos², J. A. Menking³, M. N. Dyonisius⁴, B. Bereiter^{2,5}, T. K. Bauska⁶, R. H. Rhodes⁷, E. J. Brook³, V. V. Petrenko⁴, J. R. McConnell⁸, T. Kellerhals², M. Häberli², J. Schmitt², H. Fischer² and J. P. Severinghaus¹

The Last Interglacial (129–116 thousand years ago (ka)) represents one of the warmest climate intervals of the past 800,000 years and the most recent time when sea level was metres higher than today. However, the timing and magnitude of the peak warmth varies between reconstructions, and the relative importance of individual sources that contribute to the elevated sea level (mass gain versus seawater expansion) during the Last Interglacial remains uncertain. Here we present the first mean ocean temperature record for this interval from noble gas measurements in ice cores and constrain the thermal expansion contribution to sea level. Mean ocean temperature reached its maximum value of 1.1 ± 0.3 °C warmer-than-modern values at the end of the penultimate deglaciation at 129 ka, which resulted in 0.7 ± 0.3 m of thermosteric sea-level rise relative to present level. However, this maximum in ocean heat content was a transient feature; mean ocean temperature decreased in the first several thousand years of the interglacial and achieved a stable, comparable-to-modern value by ~127 ka. The synchronicity of the peak in mean ocean temperature with proxy records of abrupt transitions in the oceanic and atmospheric circulation suggests that the mean ocean temperature maximum is related to the accumulation of heat in the ocean interior during the preceding period of reduced overturning circulation.

With a heat capacity 1,000 times larger than that of the atmosphere, the ocean plays an important role in regulating the rate and magnitude of global temperature change and represents the largest energy reservoir in the climate system¹. Ocean heat uptake and warming contribute directly to increasing sea level through thermal expansion of seawater and may play a role in future sea-level rise through enhanced shelf melting and subsequent mass loss from the Antarctic Ice Sheet². To understand the future role of ocean heat uptake, it is instructive to study the ocean temperature change during past warm periods in Earth's history.

During the Last Interglacial (LIG, 129–116 thousand years ago (ka)) surface temperatures were warmer than today, but the existing reconstructions differ substantially on the timing and magnitude of the peak warmth. A global average (land and ocean) surface temperature reconstruction³ from a compilation of seasonal and annual-average temperature records shows a maximum of 2 °C warmer temperatures during the middle of the LIG. A global annual-average sea surface temperature (SST) reconstruction⁴ shows a maximum of only 0.5 °C warmer than the preindustrial value that peaks during the earlier LIG, but is up to 1 °C warmer in the high latitudes. Climate models show considerable warmth at the mid-LIG, especially in high northern latitudes, but in line with the lack of global insolation forcing, little warming or even cooler conditions on a global scale⁵. At the same time, global sea level during the LIG was 6–9 m higher⁶. Differences in greenhouse gas and orbital forcing over the LIG relative to modern make the spatial and temporal patterns of temperature change during this period distinct from what might be expected from anthropogenic warming⁷. As a result, the LIG is not an analogue for future warming but offers a unique opportunity to assess the validity of Earth system model

predictions of sea-level rise in response to warming, provided that reliable paleoclimate data exist for model validation⁸.

Sediment cores provide valuable records of changes in ocean conditions through the LIG^{4,9–11} and are critical to understanding the spatiotemporal structure of temperature change. However, as most available records document surface ocean conditions, to deduce the total ocean heat content and thermosteric sea level from these records remains a challenge.

The measurement of atmospheric noble gases trapped in glacial ice provides a method to reconstruct changes in mean ocean temperature (MOT) independently from marine records^{12–14}. Changes in the relative atmospheric concentrations of krypton, xenon and nitrogen trace the total ocean heat content because they are caused by temperature-driven changes in gas solubilities in seawater. Here we report measurements of the ratios of Kr/N₂, Xe/N₂ and Xe/Kr in ice cores from Taylor Glacier (TG) and the EPICA Dome C (EDC) ice cores that cover the LIG and penultimate glacial, Marine Isotope Stage 6 (MIS6, 180–136 ka). We assess the timing and magnitude of ocean temperature change during the LIG and quantify the thermosteric component of the elevated sea level during this period.

Last Interglacial mean ocean temperature record

The MOT anomalies were calculated relative to the Early Holocene (11–10 ka) for each ice core because firn fractionation corrections are more robust when calculating relative MOT change compared to absolute MOT values (Supplementary information). MOT anomalies relative to the pre-industrial and modern values were subsequently calculated using the existing West Antarctic Ice Sheet (WAIS) Divide¹² and EDC¹⁵ Holocene-to-pre-industrial MOT records and pre-industrial-to-modern simulations of ocean

¹Scripps Institution of Oceanography, University of California, San Diego, La Jolla, CA, USA. ²Climate and Environmental Physics, Physics Institute and Oeschger Center for Climate Change Research, University of Bern, Bern, Switzerland. ³College of Earth, Ocean, and Atmospheric Sciences, Oregon State University, Corvallis, OR, USA. ⁴Earth & Environmental Sciences, University of Rochester, Rochester, NY, USA. ⁵Laboratory for Air Pollution / Environmental Technology, Empa, Dübendorf, Switzerland. ⁶British Antarctic Survey, Cambridge, UK. ⁷Department of Earth Sciences, University of Cambridge, Cambridge, UK. ⁸Division of Hydrologic Sciences, Desert Research Institute, Reno, NV, USA. *e-mail: sshackle@ucsd.edu

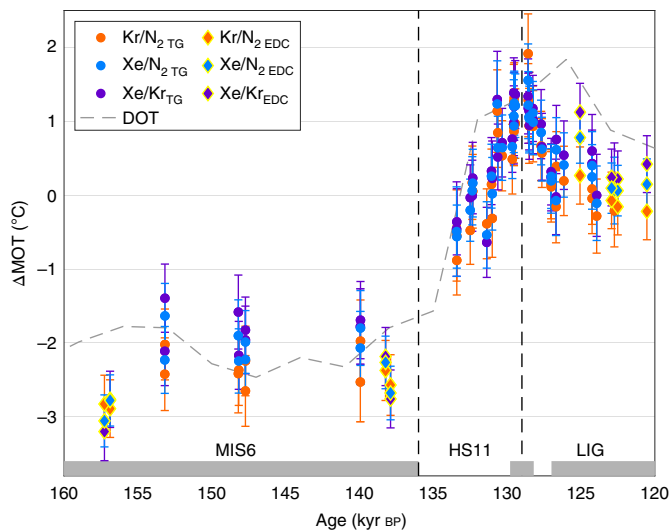


Fig. 1 | MOT anomaly from Kr/N₂, Xe/N₂ and Xe/Kr. MOT data are shown with 1σ error (Methods). The grey bars indicate the time intervals for which MIS6 MOT (>136 ka), peak MOT (129.0 ± 0.8 ka) and stable LIG MOT (<127 ka) are calculated. MOT is reported on the AICC2012 (ref. ¹⁷) chronology. Global average deep ocean temperature (DOT) from stacked marine sediment records¹¹ on LR04 (ref. ⁴²) is shown for reference. kyr, thousand years.

temperature change¹⁶. Based on Monte Carlo simulations that account for all the known sources of uncertainty (Methods), we constrained peak MOT to 1.1 ± 0.3 °C (1σ) warmer than modern at 129.0 ± 0.8 ka on the Antarctic Ice Core Chronology (AICC2012)¹⁷ (Fig. 1). Although data for MIS6 and Termination II are relatively sparse, the period of maximum MOT is highly resolved (Methods). This and the robust age constraints from trace gas measurements for the TG record (Methods and Supplementary information) mean that the timing of the peak MOT is well-constrained.

The record shows a 3.4 ± 0.5 °C MOT increase from MIS6 to the early LIG, compared to the Last Glacial Maximum-to-Holocene change of 2.6 ± 0.3 °C (ref. ¹²). The larger magnitude in glacial–interglacial MOT change over Termination II versus Termination I is consistent with previous reconstructions of deep ocean temperature during these intervals from stacks of low-resolution marine records¹¹.

Comparison to global surface temperature records

Comparison of our MOT record to stacked SST records from marine sediments⁴ over the LIG reveals distinct differences between these fundamental climate parameters (Fig. 2). The maximum in MOT occurs earlier and exceeds the magnitude of the global SST maximum. The magnitude of the peak extratropical SST anomaly agrees well with the peak MOT anomaly, although the temporal evolution of each record over the LIG appears distinct. Comparison of the timing of the MOT and SST changes is complicated by the lack of absolute age constraints for the sediment and ice core records that span the LIG, and a 1,000–2,000-year offset between the SpeleoAge¹⁸ and AICC2012 chronologies that are applied to the SST and MOT records, respectively¹⁹. However, accounting for the offset in chronologies would actually increase the offset in the relative timing of the MOT and global SST maxima.

While global SST records are good indicators of the ‘skin temperature’ and thus outgoing long-wave radiation for much of the planet, MOT is closely related to the subsurface heat content¹⁵. MOT represents the volume-averaged ocean temperature, so changes in intermediate and deep ocean temperatures (as opposed to SST changes) play a dominant role in setting the MOT. Much of the intermediate

and deep ocean’s temperature is set at high latitudes via meridional circulation, so the polar regions are probably crucial for the structure of MOT change, relative to that of global SST²⁰.

MOT and Antarctic surface temperature²¹ records show strikingly similar features (Figs. 2 and 3). Both records are reported on AICC2012, but minor uncertainties in their alignment may result from error in the TG chronology, or the EDC gas–ice age difference²². The covariation of MOT and Antarctic temperature during the LIG follows the pattern recently observed during Termination I^{12,15} in which mean ocean and high southern latitude surface warming precede the increase in global SST and appear intrinsically linked. We thus have strong evidence that changes in MOT outpace and exceed low latitude SST changes during the LIG, which suggests that polar amplification and intermediate/deep-water formation are key regulators of MOT.

Links of MOT and ocean circulation over Termination II/LIG

Recent studies investigated the role of the bipolar seesaw, the out-of-phase temperature variations between hemispheres, in the evolution of glacial terminations^{10,18,23,24}. Although the exact triggering mechanisms are still debated, it is generally accepted that the bipolar pattern of global temperature anomalies is the result of variations in the strength of the Atlantic Meridional Overturning Circulation (AMOC)²⁵. When AMOC is in a strong mode, as today, there is a northward heat transport at all latitudes in the Atlantic. When AMOC is weakened, this heat transport is reduced, which leads to a net accumulation of heat in the Southern Hemisphere.

A recent synthesis of the available high-resolution records that cover Termination II²⁶, which includes sediment records from the North Atlantic¹⁰, Chinese speleothems²⁴ and Antarctic ice cores^{27,28}, suggests that the AMOC was considerably weakened during Heinrich Stadial 11 (HS11, ~136–129 ka), a cold period in the Northern Hemisphere that covers much of Termination II. At ~129 ka, these proxy records show a rapid recovery of the AMOC and Asian monsoon strength, which coincides with an abrupt shift in the source of Antarctic moisture²⁷, methane (CH₄) increase²⁸ and a peak in our MOT reconstruction (Fig. 3). As CH₄ and the noble gases are measured on the same ice samples, there is virtually no uncertainty in the relative timing of the abrupt rise in CH₄ and the MOT maximum (Supplementary information). The excellent agreement in the timing of the peak in MOT (129.0 ± 1.9 ka, including the AICC2012 uncertainty) and the end of HS11 (128.9 ± 0.06 ka, dated from the Sanbao Cave records²⁴) also suggests an important connection between MOT and the bipolar seesaw.

Recent modelling studies examined the impact of a reduced AMOC on the surface and subsurface temperature change through freshwater hosing experiments^{14,25,29}. In these simulations, a reduction in the AMOC strength results in a globally asymmetric surface pattern of cold Northern Hemisphere SSTs, as the Southern Hemisphere SSTs, MOT and Antarctic temperatures gradually increase. At the subsequent recovery of the AMOC, the accumulated subsurface heat is released, which leads to an abrupt increase in the Northern Hemisphere SSTs and gradual decrease in the Southern Hemisphere SSTs, Antarctic temperature and MOT²⁵. This spatio-temporal pattern is consistent with the observed Antarctic temperature and MOT trends during HS11 and the LIG (Fig. 3). As in the hosing simulations, we observe that MOT and Antarctic temperature increase during the weakened AMOC interval of HS11, reach a maximum at ~129 ka synchronous with the AMOC recovery¹⁰, and then decrease during the several thousand years after the AMOC recovery. This mechanism is also consistent with the lead of the Southern Hemisphere over the Northern Hemisphere high-latitude warming observed at the onset of the LIG^{4,9}.

These observations raise the question³⁰ of how much of the warmer-than-modern MOT in the early LIG was due to the weakened AMOC state, and how much can be attributed to the stable

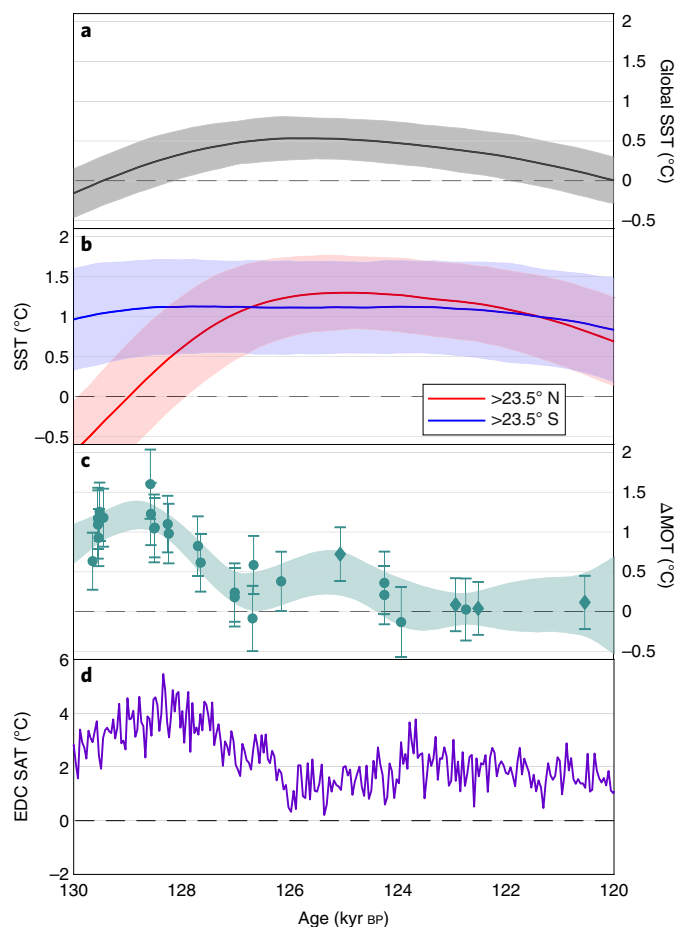


Fig. 2 | Surface and MOT anomalies during the LIG. **a, b,** Global (**a**) and extratropical (**b**) SST from the Northern Hemisphere (red) and Southern Hemisphere (blue) (relative to pre-industrial) from stacked SST proxy records⁴ on the SpeleoAge chronology¹⁸. The shading shows the 2σ confidence intervals. **c,** MOT (relative to modern) from TG (circles) and EDC (diamonds) on AICC2012 (ref. ¹⁷) with 1σ error bars and a 1σ confidence envelope (shading). **d,** EDC surface air temperature²¹ (SAT, relative to the average of the past 1,000 yr) on AICC2012.

interglacial climate. In our record, MOT decreased and eventually stabilized by ~ 127 ka (at the latest by ~ 124 ka) at a temperature that is comparable to that of the Holocene/modern MOT ($+0.2 \pm 0.3$ °C). If the observed MOT decrease was due to the release of stored heat post-AMOC recovery, then we can attribute most of the MOT anomaly at the LIG onset to deglacial changes in ocean circulation.

Although our Termination II record of MOT lacks resolution at its onset, the only observed warming occurs during the weakened AMOC interval, HS11. Northern Hemisphere insolation forcing during Termination II exceeded that of Termination I, which may, in part, explain the comparatively rapid disintegration of the Northern Hemisphere ice sheets during Termination II, and the long duration of suppressed AMOC due to strong freshwater forcing of the North Atlantic²³. During Termination I, the AMOC temporarily recovered, possibly due to weaker insolation and reduced freshwater forcing³¹. During this time, Antarctic temperatures and MOT decreased (Fig. 3). The so-called ‘Antarctic Cold Reversal’ may, in many ways, be analogous to the Antarctic and mean ocean cooling observed at the end of Termination II, post-AMOC recovery. Although the magnitude of the MOT decrease over the Antarctic Cold Reversal was slightly smaller than that observed for the LIG onset, the net mean ocean warming during Heinrich Stadial 1

(ref. ¹²) and the Younger Dryas³² of 3.4 ± 0.4 °C is remarkably similar to the net warming found from MIS6 to the LIG peak observed in our record (3.4 ± 0.5 °C). In addition, the magnitude of glacial–interglacial change across Termination II once MOT has stabilized is 2.5 ± 0.5 °C, which is comparable to the magnitude of the MOT change across Termination I (2.6 ± 0.3 °C). Several studies that compare Terminations I and II posit that the larger magnitude of changes in Antarctic temperature²⁷ and carbon dioxide (CO₂) concentration (ref. ¹⁰) across Termination II are related to the delayed recovery of the AMOC strength. Our record suggests the same is true for MOT.

These observations suggest that the AMOC interruptions during the past two terminations transiently provided an additional ~ 1 °C of mean ocean warming above the net glacial–interglacial MOT change. A recent quantitative assessment of Earth’s radiative imbalance over Termination I¹⁵ found positive maxima in the radiative imbalance during the Younger Dryas and Heinrich Stadial 1, which suggests that a reduced AMOC during these intervals contributed energy to the climate system through an increase in ocean heat storage. This storage and subsequent release of energy may play a critical role in terminations²⁹. As shown in simulations²⁹, when the AMOC is reduced, the subsurface ocean works as a ‘capacitor’, storing heat while the surface (centred on the North Atlantic) remains cold. Once the AMOC recovers, the subsurface heat is released, which enhances surface warming. Although our MOT record lacks the necessary resolution to conduct a similar assessment of the radiative imbalance across Termination II, the comparable magnitudes of the enhanced mean ocean warming during the weakened AMOC intervals over the past two terminations suggest that this mechanism was also important for Termination II. Along with the potential importance of AMOC interruptions in releasing Southern Ocean CO₂ (refs ^{33,34}) and in destabilizing the Northern Hemisphere ice sheets^{35,36}, their role in providing additional energy to the climate system lends support to the hypothesis that AMOC interruptions are not merely incidental to terminations, but play a role in driving the climate out of glacial conditions^{18,24}.

Implications for WAIS stability

The MOT changes across the LIG have direct and indirect implications for sea level. Pinning down the sources that contribute to the LIG global mean sea-level highstand is crucial to understand the vulnerability of modern ice sheets to global warming. From CMIP5 estimates of the expansion efficiency of heat (0.12 m YJ⁻¹) (ref. ³⁷), we found that the 1.1 ± 0.3 °C MOT anomaly during the early stages of the LIG contributed 0.7 ± 0.3 m to the elevated sea level. By ~ 127 ka, MOT had decreased to near-modern values with no appreciable thermosteric contribution to sea level. In fact, our record implies a trend of thermosteric sea-level lowering in the first several thousand years of the LIG. Coral reef records indicate that the sea level was already 5.9 ± 1.7 m higher than modern at 128.6 ± 0.8 ka (ref. ³⁸), which requires a substantial ice sheet (in addition to thermosteric) contribution early in the LIG to explain the magnitude of elevated sea level.

The early maximum in MOT may have played another, more indirect role in contributing to sea-level rise during the LIG. In recent Antarctic Ice Sheet simulations of the LIG^{39,40}, ocean warming played an important role in mass loss from the WAIS. Pollard and Deconto³⁹ found that if ocean warming occurred shortly after the glacial termination, the WAIS was more prone to lose mass because of enhanced reverse-sloped beds at the grounding lines. By invoking subshelf melting through Southern Ocean warming, Sutter et al.⁴⁰ derived the highest rates of sea-level rise during the maximum Antarctic temperatures at the end of Termination II, synchronous to our MOT maximum. The delay in the AMOC recovery and resulting accumulation of heat in the ocean interior and Southern Hemisphere at the end of Termination II may, therefore,

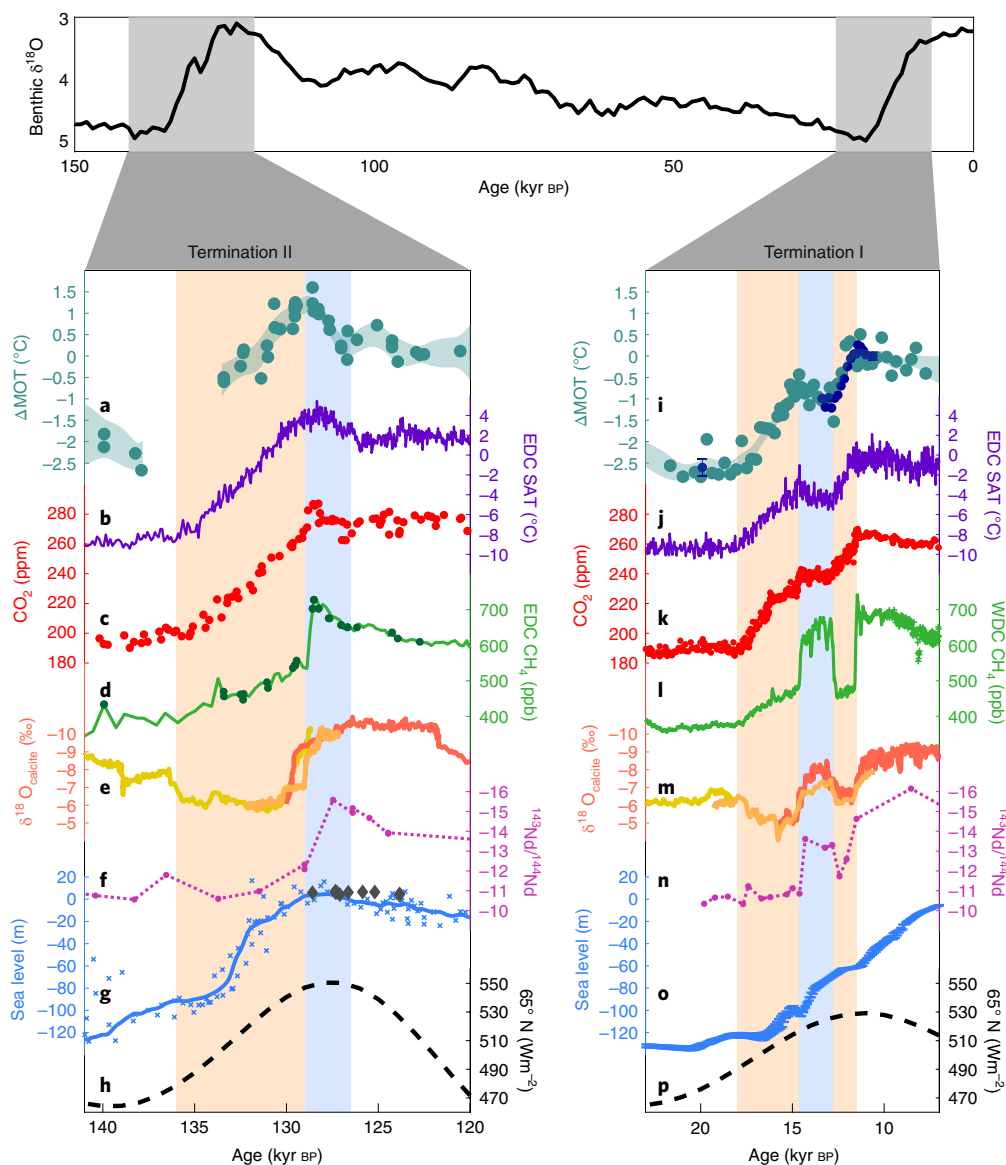


Fig. 3 | Climate records of Terminations II and I. **a–h**, Climate records of Termination II. **a**, MOT anomaly relative to modern from this study with 1σ error (shading). **b**, Antarctic temperature²¹ anomaly relative to the average over the past 1,000 yr. **c**, CO₂ (ref. 43). **d**, CH₄ (ref. 28). The green circles show TG CH₄ measurements. **a–d** are presented on AICC2012 (ref. 17). **e**, Sanbao Cave^{24,44} ²³⁰Th-dated $\delta^{18}\text{O}_{\text{calcite}}$ records. Colours distinguish the individual speleothems. **f**, North Atlantic ¹⁴³Nd/¹⁴⁴Nd (ref. 10) on a core-specific age scale. **g**, Red sea level corrected for isostatic effects⁴⁵ on a core-specific age scale (light blue). The grey diamonds show coral reef sea-level records³⁸. **h**, Summer solstice insolation at 65°N. **i–p**, Climate records of Termination I. **i**, MOT anomaly relative to modern from the WAIS Divide (WDC)¹² (turquoise) and TG³² (dark blue). Error bars show the spread (1σ) of TG replicate samples measured at Scripps Institution of Oceanography (SIO) for this study (Supplementary Information). **j**, As in **b** but for Termination I. **k**, CO₂ (ref. 46). **l**, CH₄ (ref. 47). **i, k** and **l** are presented on WD2014 (ref. 48). **m**, Dongge Cave⁴⁹ (red) and Hulu⁵⁰ (orange and yellow) $\delta^{18}\text{O}_{\text{calcite}}$ records. **n**, North Atlantic ¹⁴³Nd/¹⁴⁴Nd (ref. 51) on core-specific age scale. **o**, Eustatic sea level⁵² with 1σ error from radiocarbon/uranium series-dated coral and sediment records. **p**, As for **h**. The orange bars indicate the times when the AMOC was in a weakened mode and the blue bars show periods of strong AMOC and mean ocean/Antarctic cooling. Top panel: benthic $\delta^{18}\text{O}$ on LR04⁴². The grey bars highlight the intervals shown in **a–p**.

have played an important role in WAIS mass loss and elevated sea level during the LIG.

An important caveat to consider for this hypothesis is that MOT is not a proxy for ocean temperatures directly under ice shelves, and a higher MOT does not necessarily imply that temperatures in vulnerable sub-ice-shelf regions were enhanced. However, MOT and the temperature of the circumpolar deep water are intrinsically linked because circumpolar deep water is made up of a representative mixture of waters from all the ocean basins⁴¹ and is brought efficiently to the surface by isopycnal mixing in the Southern Ocean. If, as today, circumpolar deep water intruded onto the Antarctic

continental shelf, its ice melting capacity would be enhanced during the early stages of the LIG.

Conclusions

The ocean heat anomaly provided from our MOT reconstruction is a simple but important metric to evaluate in Earth system models, which makes it useful for forthcoming simulations of the LIG. Comparison with other proxy and model results suggest that peak MOT coincided with the abrupt recovery of the AMOC at the end of Termination II and was a transient rather than stable feature of the LIG. An enhanced MOT contributed to elevated thermoseric

sea level during the early stages of the LIG and may have played a more indirect role in the sea-level highstand through amplified melting of ice sheets and shelves from below. The temporal evolution of the AMOC and MOT over the past two terminations suggests that the ocean's overturning circulation plays a dominant role in controlling the timing and magnitude of MOT change across terminations; studying the LIG in the context of the termination that preceded it provides a more complete view of the climate evolution that occurred over this interval.

Online content

Any methods, additional references, Nature Research reporting summaries, source data, extended data, supplementary information, acknowledgements, peer review information; details of author contributions and competing interests; and statements of data and code availability are available at <https://doi.org/10.1038/s41561-019-0498-0>.

Received: 9 June 2019; Accepted: 6 November 2019;

Published online: 6 January 2020

References

- IPCC *Climate Change 2013: The Physical Science Basis* (eds Stocker, T. F. et al.) (Cambridge Univ. Press, 2013).
- Pritchard, H. D. et al. Antarctic ice-sheet loss driven by basal melting of ice shelves. *Nature* **484**, 502–505 (2012).
- Snyder, C. W. Evolution of global temperature over the past two million years. *Nature* **538**, 226–228 (2016).
- Hoffman, J. S., Parnell, A. C. & He, F. Regional and global sea-surface temperatures during the last interglaciation. *Science* **279**, 276–279 (2017).
- Otto-Bliesner, B. L. et al. How warm was the Last Interglacial? New model—data comparisons. *Philos. Trans. R. Soc. A* **371**, 20130097 (2013).
- Kopp, R. E., Simons, F. J., Mitrovica, J. X., Maloof, A. C. & Oppenheimer, M. Probabilistic assessment of sea level during the Last Interglacial stage. *Nature* **462**, 863–867 (2009).
- Masson-Delmotte, V. et al. Sensitivity of interglacial Greenland temperature and $\delta^{18}\text{O}$: ice core data, orbital and increased CO_2 climate simulations. *Clim. Past* **7**, 1041–1059 (2011).
- Fischer, H. et al. Palaeoclimate constraints on the impact of 2 °C anthropogenic warming and beyond. *Nat. Geosci.* **11**, 475–485 (2018).
- Capron, E. et al. Temporal and spatial structure of multi-millennial temperature changes at high latitudes during the Last Interglacial. *Quat. Sci. Rev.* **103**, 116–133 (2014).
- Deaney, E., Barker, S. & van de Fliedert, T. Timing and nature of AMOC recovery across Termination 2 and magnitude of deglacial CO_2 change. *Nat. Commun.* **8**, 14595 (2017).
- Shakun, J. D., Lea, D. W., Lisiecki, L. E. & Raymo, M. E. An 800-kyr record of global surface ocean $\delta^{18}\text{O}$ and implications for ice volume-temperature coupling. *Earth Planet. Sci. Lett.* **426**, 58–68 (2015).
- Bereiter, B., Shackleton, S., Baggenstos, D., Kawamura, K. & Severinghaus, J. Mean global ocean temperatures during the last glacial transition. *Nature* **553**, 39–44 (2018).
- Headly, M. A. & Severinghaus, J. P. A method to measure Kr/N_2 ratios in air bubbles trapped in ice cores and its application in reconstructing past mean ocean temperature. *J. Geophys. Res.* **112**, D19105 (2007).
- Ritz, S. P., Stocker, T. F. & Severinghaus, J. P. Noble gases as proxies of mean ocean temperature: sensitivity studies using a climate model of reduced complexity. *Quat. Sci. Rev.* **30**, 3728–3741 (2011).
- Baggenstos, D. et al. The Earth's radiative imbalance from the Last Glacial Maximum to the present. *Proc. Natl Acad. Sci. USA* **116**, 14881–14886 (2019).
- Gebbie, G. & Huybers, P. The Little Ice Age and 20th-century deep Pacific cooling. *Science* **363**, 70–74 (2019).
- Bazin, L. et al. An optimized multi-proxy, multi-site Antarctic ice and gas orbital chronology (AICC2012): 120–800 ka. *Clim. Past* **9**, 1715–1731 (2013).
- Barker, S. et al. 800,000 years of abrupt climate variability. *Science* **334**, 347–352 (2011).
- Capron, E., Govin, A., Feng, R., Otto-Bliesner, B. L. & Wolff, E. W. Critical evaluation of climate syntheses to benchmark CMIP6/PMIP4 127 ka Last Interglacial simulations in the high-latitude regions. *Quat. Sci. Rev.* **168**, 137–150 (2017).
- Gebbie, G. & Huybers, P. How is the ocean filled? *Geophys. Res. Lett.* **38**, L06604 (2011).
- Jouzel, J. et al. Orbital and millennial Antarctic climate variability over the past 800,000 years. *Science* **317**, 793–796 (2007).
- Parrenin, F. et al. On the gas–ice depth difference (Δ depth) along the EPICA Dome C ice core. *Clim. Past* **8**, 1239–1255 (2012).
- Marino, G. et al. Bipolar seesaw control on Last Interglacial sea level. *Nature* **522**, 197–201 (2015).
- Cheng, H. et al. Ice Age terminations. *Science* **326**, 248–252 (2009).
- Pedro, J. B. et al. Beyond the bipolar seesaw: toward a process understanding of interhemispheric coupling. *Quat. Sci. Rev.* **192**, 27–46 (2018).
- Menviel, L. et al. The penultimate deglaciation: protocol for Paleoclimate Modelling Intercomparison Project (PMIP) phase 4 transient numerical simulations between 140 and 127 ka, version 1.0. *Geosci. Model Dev. Discuss.* **10**, 3649–3685 (2019).
- Masson-Delmotte, V. et al. Abrupt change of Antarctic moisture origin at the end of Termination II. *Proc. Natl Acad. Sci. USA* **107**, 10–13 (2010).
- Loulergue, L. et al. Orbital and millennial-scale features of atmospheric CH_4 over the past 800,000 years. *Nature* **453**, 383–386 (2008).
- Galbraith, E. D., Merlis, T. M. & Palter, J. B. Destabilization of glacial climate by the radiative impact of Atlantic meridional overturning circulation disruptions. *Geophys. Res. Lett.* **43**, 8214–8221 (2016).
- Barker, S. et al. Early interglacial legacy of deglacial climate instability. *Paleoceanogr. Paleoclimatol.* **34**, 1455–1475 (2019).
- Carlson, A. E. Why there was not a Younger Dryas-like event during the penultimate deglaciation. *Quat. Sci. Rev.* **27**, 882–887 (2008).
- Shackleton, S. et al. Is the noble gas-based rate of ocean warming during the younger dryas overestimated? *Geophys. Res. Lett.* **46**, 5928–5936 (2019).
- Anderson, R. F. et al. Wind-driven upwelling in the Southern Ocean and the deglacial rise in atmospheric CO_2 . *Science* **323**, 1443–1448 (2009).
- Toggweiler, J. R., Russell, J. L. & Carson, S. R. Midlatitude westerlies, atmospheric CO_2 , and climate change during the ice ages. *Paleoceanography* **21**, PA2005 (2006).
- Marcott, S. A. et al. Ice-shelf collapse from subsurface warming as a trigger for Heinrich events. *Proc. Natl Acad. Sci. USA* **108**, 13415–13419 (2011).
- Bassis, J., Petersen, S. & Mac Cathles, L. Heinrich events triggered by ocean forcing and modulated by isostatic adjustment. *Nature* **542**, 332–334 (2017).
- Kuhlbrodt, T. & Gregory, J. M. Ocean heat uptake and its consequences for the magnitude of sea level rise and climate change. *Geophys. Res. Lett.* **39**, L18608 (2012).
- Dutton, A., Webster, J. M., Zwartz, D. & Lambeck, K. Tropical tales of polar ice: evidence of Last Interglacial polar ice sheet retreat recorded by fossil reefs of the granitic Seychelles islands. *Quat. Sci. Rev.* **107**, 182–196 (2015).
- Pollard, D. & Deconto, R. M. Contribution of Antarctica to past and future sea-level rise. *Nature* **531**, 591–597 (2016).
- Sutter, J., Gierz, P., Grosfeld, K., Thoma, M. & Lohmann, G. Ocean temperature thresholds for Last Interglacial West Antarctic Ice Sheet collapse. *Geophys. Res. Lett.* **43**, 2675–2682 (2016).
- Schneider, R., Schmitt, J., Köhler, P., Joos, F. & Fischer, H. A reconstruction of atmospheric carbon dioxide and its stable carbon isotopic composition from the penultimate glacial maximum to the last glacial inception. *Clim. Past* **9**, 2507–2523 (2013).
- Wang, Y. et al. Millennial- and orbital-scale changes in the East Asian monsoon over the past 224,000 years. *Nature* **451**, 1090–1093 (2008).
- Grant, K. M. et al. Sea-level variability over five glacial cycles. *Nat. Commun.* **5**, 5076 (2014).
- Marcott, S. A. et al. Centennial-scale changes in the global carbon cycle during the last deglaciation. *Nature* **514**, 616–619 (2014).
- Buizert, C. et al. Precise interproxy phasing of abrupt climate change during the last ice age. *Nature* **520**, 661–665 (2015).
- Buizert, C. et al. The WAIS-Divide deep ice core WD2014 chronology—part 1: methane synchronization (68–31 ka bp) and the gas age-ice age difference. *Clim. Past* **11**, 153 (2015).
- Dykoski, C. A. et al. A high-resolution, absolute-dated Holocene and deglacial Asian monsoon record from Dongge Cave, China. *Earth Planet. Sci. Lett.* **233**, 71–86 (2005).
- Wang, Y. et al. A high-resolution absolute-dated Late Pleistocene monsoon record from Hulu Cave, China. *Science* **294**, 2345–2348 (2001).
- Roberts, N. L., Piotrowski, A. M., McManus, J. F. & Keigwin, L. D. Synchronous deglacial overturning and water mass source changes. *Science* **327**, 75–78 (2010).
- Elderfield, H. et al. Evolution of ocean temperature and ice volume through the mid-Pleistocene climate transition. *Science* **337**, 704–709 (2012).
- Lisiecki, L. E. & Raymo, M. E. A Pliocene–Pleistocene stack of 57 globally distributed benthic $\delta^{18}\text{O}$ records. *Paleoceanography* **20**, PA1003 (2005).
- Lambeck, K., Rouby, H., Purcell, A., Sun, Y. & Sambridge, M. Sea level and global ice volumes from the Last Glacial Maximum to the Holocene. *Proc. Natl Acad. Sci. USA* **111**, 15296–15303 (2014).

Publisher's note Springer Nature remains neutral with regard to jurisdictional claims in published maps and institutional affiliations.

This is a U.S. government work and not under copyright protection in the U.S.; foreign copyright protection may apply 2020

Methods

Taylor Glacier sampling and site description. TG is an outlet glacier of the East Antarctic Ice Sheet with a >80 km long ablation zone that exposes easily accessible old ice at the surface. Its accumulation zone is located on the northern flank of Taylor Dome and it terminates in Taylor Valley. Extensive work on mapping the stratigraphy of the glacier identified ice from the LIG located near the terminus of the glacier^{53–55}.

For this study, four large-diameter ice cores were collected during the 2014/2015 and 2015/2016 Antarctic field seasons (Supplementary Fig. 1). Two cores that span approximately 155–120 ka were collected approximately 4 km from the glacier terminus. Additionally, two cores were drilled along a previously established cross-flow transect⁵³ from the early Holocene (10.6 ka) and Last Glacial Maximum (19.9 ka) to serve as a comparison to the LIG and MIS6 MOT samples. Cores were drilled with the Blue Ice Drill⁵⁶ and are 24.1 cm in diameter. Cores were processed and subdivided in the field and analysed in the lab for noble gases for the MOT reconstruction as well as for other atmospheric gases used to establish the chronology of the record.

Taylor Glacier core chronology. A major challenge in sampling a blue ice area is to establish the ages of the samples⁵⁷. Ice from TG has travelled tens of kilometres from its deposition site and has probably undergone non-uniform thinning and folding. Although the dynamics of the glacier have been studied in detail^{58,59}, not enough is known about the basal topography or subsurface ice flow to build a chronology for the glacier from a glaciological model.

We therefore used alternative methods to construct the chronology for our samples. Previous work in blue ice areas^{53,60–62} demonstrated success in establishing ice sample chronologies through value and/or inflection point matching of well-mixed atmospheric gases to well-dated ice-core records⁶³. For this study, the chronology was constructed using a least-squares fitting method with measurements of CH₄ concentrations, molecular oxygen isotopic composition ($\delta^{18}\text{O}_{\text{atm}}$) and CO₂ concentrations, tied to EDC reference records^{28,43,64} on AICC2012^{17,65}. This method allows for a construction of an age probability distribution for each noble gas sample that can be used to assess the sample age uncertainty (Supplementary information).

Taylor Glacier noble gas measurements. TG measurements of noble gases for the MOT reconstruction were made at SIO. A total of 45 ice samples from the 2014/2015 and 2015/2016 cores were analysed, which included 8 replicate samples to give 37 unique MOT samples. Of the 45 samples, 3 were rejected due to sample age uncertainty (Supplementary information). In addition, five samples from the Holocene (10.6 ka) and five from the Last Glacial Maximum (19.9 ka) were measured (Fig. 3) at both SIO and Bern. The motivation for this analysis was to verify the quality of the noble gas records by comparison to published MOT records¹², and to verify that any offsets in the EDC and TG MOT results were unrelated to lab offsets (Supplementary information).

The analytical methods for the noble gas measurements are described in detail by Bereiter et al.⁶⁶. In short, ~800 g of ice were melted under vacuum and the liberated gases (~80 ml at standard temperature and pressure (STP)) were cryogenically trapped in stainless-steel dip tubes. After gas extraction, the samples were split into two aliquots. The larger aliquot (~78 ml STP) was exposed to a Zr/Al alloy at 900 °C to remove all the non-noble gases and measured on a Thermo-Finnigan MAT-253 isotope ratio mass spectrometer via a dual inlet method for ⁴⁰Ar/³⁸Ar ($\delta^{40/38}\text{Ar}$), ⁴⁰Ar/³⁶Ar ($\delta^{40/36}\text{Ar}$), ⁸⁶Kr/⁸⁴Kr ($\delta^{86/84}\text{Kr}$), ⁸⁶Kr/⁸³Kr ($\delta^{86/83}\text{Kr}$), ⁸⁶Kr/⁸²Kr ($\delta^{86/82}\text{Kr}$), ⁸⁴Kr/⁴⁰Ar ($\delta\text{Kr}/\text{Ar}$) and ¹³²Xe/⁴⁰Ar ($\delta\text{Xe}/\text{Ar}$). The smaller aliquot (~2 ml STP) was passed through a cryotrap (–196 °C) to remove CO₂ and measured on a Thermo-Finnigan MAT Delta V isotope ratio mass spectrometer via a dual inlet method for ²⁹N₂/²⁸N₂ ($\delta^{15}\text{N}$), ³⁴O₂/³²O₂ ($\delta^{18}\text{O}$), ³²O₂/²⁸N₂ ($\delta\text{O}_2/\text{N}_2$) and ⁴⁰Ar/²⁸N₂ ($\delta\text{Ar}/\text{N}_2$). Measurements were corrected for pressure imbalance and chemical slope according to established procedures⁶⁷.

All data are reported in delta notation relative to a modern atmosphere standard. As argon is preferentially lost relative to xenon and krypton during ice bubble formation⁶⁸, we mathematically combine $\delta\text{Xe}/\text{Ar}$, $\delta\text{Kr}/\text{Ar}$ and $\delta\text{Ar}/\text{N}_2$ to obtain $\delta\text{Kr}/\text{N}_2$, $\delta\text{Xe}/\text{N}_2$ and $\delta\text{Xe}/\text{Kr}$.

Taylor Glacier fractionation corrections. To reconstruct ocean temperatures from Kr/N₂, Xe/N₂ and Xe/Kr, it is necessary to correct for fractionation during firnification, the process by which fresh snow compacts, transitioning to denser firn and eventually to glacial ice containing air trapped in bubbles. Although the free troposphere is well-mixed through convective processes, the low permeability of the firn restricts bulk flow; gases within the firn column are transported primarily via molecular diffusion⁶⁹. This allows gravitational settling and thermal diffusion to alter the firn air from its atmospheric composition before it is occluded in glacial ice^{70,71}. As such, Kr/N₂, Xe/N₂ and Xe/Kr must be corrected for the fractionating processes to derive the palaeoatmospheric composition for inferring MOT.

As suggested by Bereiter et al.¹², under- or overcorrection of the fractionation may lead to systematic offsets in MOT, but the effect primarily impacts the absolute MOT anomaly (relative to modern) and has little impact on the relative MOT change within a record. We investigated the influence of the choice in the

methods of fractionation correction on the MOT record and found that different methods shifted the absolute MOT record up or down but had little effect on the relative MOT change in the TG record (Supplementary information). We thus computed the MOT anomalies relative to the TG Holocene (10.6 ka) samples, and then estimated the Holocene–modern MOT difference (and uncertainties) from the WAIS Divide MOT record and model simulations of ocean heat content over the past 2,000 yr (ref. 16). A detailed description and assessment of the fractionation corrections is included in the Supplementary information.

EDC ice-core noble gas analysis. Four EDC ice-core samples from the LIG and four from MIS6 were analysed at the University of Bern and included in this study. The measurement and data processing for these samples are similar to the analysis of TG samples with a few important distinctions (Baggenstos et al.¹³ and Supplementary information). Chronological uncertainties were not considered in this analysis, because the TG chronology is tied to that of EDC through ice-core synchronization and contribute minimally to the total uncertainty for these samples. In addition, the approach to firn fractionation corrections differs slightly between TG and EDC (Supplementary Section 4).

Derivation of MOT from noble gas data. To reconstruct the MOT values from fractionation-corrected Kr/N₂, Xe/N₂ and Xe/Kr, we used the ocean–atmosphere box model of Bereiter et al.¹² with several modifications. We made no assumptions about the glacial–interglacial change in the ocean saturation state and used current estimates of krypton and xenon undersaturation⁷² in the box model for the entirety of the record. We also did not invoke the glacial–interglacial changes in the relative water mass distributions that were applied in Bereiter et al.¹² and used the modern distributions of Antarctic Bottom Water and North Atlantic Deep Water to derive MOT over the full record.

We accounted for the effects of changes in ocean salinity, volume and atmospheric pressure on the oceanic inventories of krypton, xenon and nitrogen using the sea-level record of Toggweiler et al.³⁴ corrected for isostatic effects (Supplementary information). We also included the influence of a large ice shelf over the Arctic during MIS6, which holds the equivalent of 15 m of sea level, affecting ocean salinity and volume, but not sea level⁷³.

To assess uncertainty in our MOT record, we ran 10,000 Monte Carlo simulations of our reconstruction with all the known analytical and dating uncertainties in the MOT and sea-level records, as well as the uncertainty in the Holocene-to-modern MOT change. We included uncertainties in the measured Kr/N₂, Xe/N₂ and Xe/Kr and the isotope data used to correct for firn processes in our simulations, as well as the method used for fractionation corrections (Supplementary Section 4). To account for age uncertainties in the MOT record, we used an inverse transform method⁷⁴ to randomly sample from our age probability distribution to use in our Monte Carlo simulations. For our final uncertainty estimate, we used the average of the three MOT records (and the Monte Carlo simulations) from Kr/N₂, Xe/N₂ and Xe/Kr to minimize the influence of analytical noise from any single measurement.

The 1 σ confidence envelope shown in Figs. 2 and 3 was constructed using the MATLAB cubic smoothing spline function (csaps) with a 2,500 yr cutoff period on the 10,000 Monte Carlo MOT reconstructions. Each reconstruction was resampled using a bootstrapping method before the spline was produced. The 1 σ confidence envelope was then calculated from the distribution of the Monte Carlo splines at each time interval in the record.

Data availability

The presented data are available online at www.usap-dc.org/view/dataset/601218.

References

- Baggenstos, D. et al. Atmospheric gas records from Taylor Glacier, Antarctica, reveal ancient ice with ages spanning the entire last glacial cycle. *Clim. Past* **13**, 943–958 (2017).
- Buizert, C. et al. Radiometric ⁸¹Kr dating identifies 120,000-year-old ice at Taylor Glacier, Antarctica. *Proc. Natl Acad. Sci. USA* **111**, 6876–6881 (2014).
- Aarons, S. M., Aciego, S. M., McConnell, J. R., Delmonte, B. & Baccolo, G. Dust transport to the Taylor Glacier, Antarctica during the last interglacial. *Geophys. Res. Lett.* **46**, 2261–2270 (2019).
- Kuhl, T. W. et al. A new large-diameter ice-core drill: The Blue Ice Drill. *Ann. Glaciol.* **55**, 1–6 (2014).
- Bintanja, R. On the glaciological, meteorological, and climatological significance of Antarctic blue ice areas. *Rev. Geophys.* **37**, 337–359 (1999).
- Aciego, S. M., Cuffey, K. M., Kavanaugh, J. L., Morse, D. L. & Severinghaus, J. P. Pleistocene ice and paleo-strain rates at Taylor Glacier, Antarctica. *Quat. Res.* **68**, 303–313 (2007).
- Kavanaugh, J. L. & Cuffey, K. M. Dynamics and mass balance of Taylor Glacier, Antarctica: 2. Force balance and longitudinal coupling. *J. Geophys. Res.* **114**, F04011 (2009).
- Petrenko, V. V., Severinghaus, J. P., Brook, E. J., Reeh, N. & Schaefer, H. Gas records from the West Greenland ice margin covering the Last Glacial Termination: a horizontal ice core. *Quat. Sci. Rev.* **25**, 865–875 (2006).

61. Bauska, T. K. et al. Carbon isotopes characterize rapid changes in atmospheric carbon dioxide during the last deglaciation. *Proc. Natl Acad. Sci. USA* **113**, 3465–3470 (2016).
62. Menking, J. A. et al. Spatial pattern of accumulation at Taylor Dome during Marine Isotope Stage 4: stratigraphic constraints from Taylor Glacier. *Clim. Past* **15**, 1537–1556 (2019).
63. Blunier, T. et al. Synchronization of ice core records via atmospheric gases. *Clim. Past* **3**, 325–330 (2007).
64. Landais, A. et al. Two-phase change in CO₂, Antarctic temperature and global climate during Termination II. *Nat. Geosci.* **6**, 1062–1065 (2013).
65. Veres, D. et al. The Antarctic ice core chronology (AICC2012): an optimized for the last 120 thousand years. *Clim. Past* **9**, 1733–1748 (2013).
66. Bereiter, B., Kawamura, K. & Severinghaus, J. P. New methods for measuring atmospheric heavy noble gas isotope and elemental ratios in ice core samples. *Rapid Commun. Mass Spectrom.* **32**, 801–814 (2018).
67. Severinghaus, J. P., Grachev, A., Luz, B. & Caillon, N. A method for precise measurement of argon 40/36 and krypton/argon ratios in trapped air in polar ice with applications to past firn thickness and abrupt climate change in Greenland and at Siple Dome, Antarctica. *Geochim. Cosmochim. Acta* **67**, 325–343 (2003).
68. Severinghaus, J. P. & Battle, M. O. Fractionation of gases in polar ice during bubble close-off: new constraints from firn air Ne, Kr and Xe observations. *Earth Planet. Sci. Lett.* **244**, 474–500 (2006).
69. Schwander, J., Stauffer, B. & Sigg, A. Air mixing in firn and the age of the air at pore close-off. *Ann. Glaciol.* **10**, 141–145 (1988).
70. Schwander, J. in *The Environmental Record in Glaciers and Ice Sheets* (eds Oeschger, H. & Langway, C. C.) 53–67 (Wiley, 1989).
71. Severinghaus, J. P., Sowers, T., Brook, E. J., Alley, R. B. & Bender, M. L. Timing of abrupt climate change at the end of the Younger Dryas interval from thermally fractionated gases in polar ice. *Nature* **391**, 141–146 (1998).
72. Hamme, R. C. & Severinghaus, J. P. Trace gas disequilibria during deep-water formation. *Deep Sea Res.* **54**, 939–950 (2007).
73. Nilsson, J. et al. Ice-shelf damming in the glacial Arctic Ocean: dynamical regimes of a basin-covering kilometre-thick ice shelf. *Cryosphere* **11**, 1745–1765 (2017).
74. Kolmogorov, A. N. *Foundations of the Theory of Probability* (Chelsea Publishing Co., 1950).

Acknowledgements

This research was supported by NSF grants 1246148 (SIO), 1245821 (OSU) and 1245659 (UR). We thank K. Schroeder, M. Jayred, P. Sperlich, I. Vimont, J. Ward, H. Roop, P. Neff and A. Smith for their invaluable field support for this project. Ice Drilling Design and Operations (IDDO) provided drilling support, and the US Antarctic Program provided logistical support for this project. Thanks to R. Beaudette for lab support at SIO, to M. Kalk for CO₂ measurements at OSU and to M. Arienzo and N. Chellman for their heroic operation of the continuous melting system at DRI. The research at the University of Bern that led to these results received funding from the European Research Council (ERC) under the European Union's Seventh Framework Programme FP7/2007–2013 ERC Grant 226172 (ERC Advanced Grant Modern Approaches to Temperature Reconstructions in polar Ice Cores (MATRICs)) and the Swiss National Science Foundation (200020_172506 (iCEP), 200021_155906 (NOTICE)). The EDC samples were obtained under the framework of EPICA, a joint European Science Foundation/European Commission scientific program funded by the European Union and national contributions from Belgium, Denmark, France, Germany, Italy, the Netherlands, Norway, Sweden, Switzerland and the United Kingdom. The main logistic support was provided by IPEV and PNRA at Dome C.

Author contributions

J.P.S. and S.S. designed the research. S.S., M.H., D.B. and T.K. performed the noble gas measurements. J.A.M., E.J.B., R.H.R., J.R.M. and S.S. performed the trace gas field/lab measurements for the TG age model. S.S., D.B., J.A.M., M.N.D., B.B., T.K.B., R.H.R., E.J.B., V.V.P., M.J.R., T.K., M.H., J.S., H.F. and J.P.S. analysed the data. S.S. wrote the paper with input from all the authors.

Competing interests

The authors declare no competing interests.

Additional information

Supplementary information is available for this paper at <https://doi.org/10.1038/s41561-019-0498-0>.

Correspondence and requests for materials should be addressed to S.S.

Peer review information Primary Handling Editor: James Super

Reprints and permissions information is available at www.nature.com/reprints.